

Carbon/polymer bilayer-coated Si-SiO_x electrodes with enhanced electrical conductivity and structural stability

Junpo Guo^{a,1}, Guangming Zhao^{b,1}, Tian Xie^a, Dongqi Dong^a, Chuanli Ma^a, Linghao Su^a, Liangyu Gong^a, Xiangdong Lou^c, Xuyun Guo^b, Jie Wang^{a,b,*}, Ye Zhu^{b,*}

^a College of Chemistry and Pharmaceutical Sciences, Qingdao Agricultural University, Qingdao, 266109, China.

^b Department of Applied Physics, The Hong Kong Polytechnic University, Hung Hom, Kowloon, Hong Kong, China.

^c School of Chemistry and Chemical Engineering, Henan Normal University, Xinxiang, 453007, China.

Abstract

Si-based electrodes offer exceptionally high capacity and energy density for lithium-ion batteries (LIBs), but suffer poor structural stability and low electrical conductivity that hamper their practical applications. To tackle these obstacles, we design a bilayer coating strategy and successfully demonstrate it on Si-SiO_x micro-particles: a C coating is used to improve electrical conductivity, outside which a high-strength polymer matrix composite, the C-nanoparticle-reinforced polypyrrole (CNP-PPy), is deposited to minimize the volumetric expansion of Si-SiO_x and enhance the structural stability during battery operation. Electrodes made of such robust Si-SiO_x@C/CNP-PPy micro-particles exhibit excellent cycling performance: 83% capacity retention (794 mAh/g) at 2 C rate after over 900 charging/discharging cycles for a coin-type half cell, and 80% capacity retention (with initial energy density of 308 Wh/kg) after over 1100 cycles for a pouch-type full cell. By comparing the samples with different coatings, an in-depth understanding of the performance enhancement mechanism is achieved, in which the PPy coating strengthened by both the well-dispersed CNPs and the crosslink bonding formed

¹ These authors contributed equally to this work.

* Corresponding authors.

E-mail addresses: wangjie@qau.edu.cn (J. Wang), yezhu@polyu.edu.hk (Y. Zhu)

between coatings plays the key role for the improved structural stability. Moreover, a full battery using the Si-SiO_x@C/CNP-PPy electrode successfully drives a car model, demonstrating a bright application prospect of the C/polymer bilayer coating strategy to make future commercial LIBs with high stability and energy density.

Keywords: Si-based electrode; Lithium ion battery (LIB); Bilayer; C coating; C nanoparticle reinforced polypyrrole; Polymer matrix composite.

1. Introduction

Lithium ion batteries (LIBs) with higher energy density have been replacing conventional Ni-Cd and lead-acid batteries. Currently, the energy density of LIBs is still increasing at an average rate of ~5 Wh/kg per year, making them dominant in the markets for portable electronics and electric vehicles [1]. On the other hand, the ever-increasing demand for higher capacity and energy density in various applications of energy storage and conversion devices (e.g., rechargeable battery for vehicle electrification) has already surpassed the stepwise improvement of LIBs. Hence, novel electrode materials with higher specific capacities than conventional graphite C (372 mAh/g) have attracted great attention, such as metal oxides (> 700 mAh/g [2-6]) and Si-based materials (e.g., Li₁₅Si₄, 3579 mAh/g [7-11]). Among all sorts of anode materials, Si has been extensively researched because of its high reversible capacity and low working potential (about 0.2 V vs. Li/Li⁺ [12-16]). Unfortunately, Si anodes suffer large volumetric expansion (about 300%) during cycling, which incurs a number of issues including irreversible structural failure, unstable solid electrolyte interphases (SEIs), substantial Li⁺ consumption, and severe decay of battery performance [17, 18].

As a promising alternative to Si, SiO_x not only features high theoretical specific capacity but relatively small volumetric expansion; for example, when $x = 1$ (SiO), the specific capacity is calculated to be 2323 mAh/g, and the reported volumetric expansion

is about 100% [19, 20]. According to recent research, SEI layers composed of lithium oxides or lithium silicates can form on the surface of SiO_x anodes during the first a few cycles, which are capable of limiting and buffering the volumetric expansion [21-23]. Nevertheless, SiO_x anodes have issues too, namely, poor electrical conductivity and low initial Coulombic efficiency (CE). Many efforts have been devoted to improve the Si-based electrodes through additional coating(s) [18, 19, 24-28], adding nanoparticles (NPs) or nanowires [18, 28-33], or combining with other elements [14, 34-38]. Among these attempts, C coating is an effective and low-cost approach to provide stable electrical contacts and electrode/electrolyte interfaces [24-28, 32, 39, 40]. However, C coating alone is unable to sustain the stress generated over charging/discharging cycles [41-43].

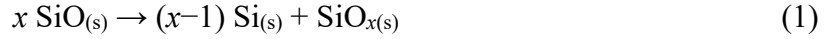
In order to address aforementioned issues of Si-based electrodes, we design a bilayer coating strategy with a high-strength polymer matrix composite (PMC) deposited outside the inner C coating. The strong crosslink bonding formed between coatings, coupled with the reinforcement of well-dispersed C nanoparticles (CNPs), results in a high-strength PMC that can effectively confine and buffer the volumetric expansion of Si-based electrodes during battery operation, thus significantly enhancing structural stability. Applying this strategy to Si- SiO_x micro-particles, we fabricate Si- SiO_x @C/PMC electrodes with excellent half-cell performance and the best ever-reported full-cell cycling stability. Systematic battery performance and microstructure characterizations are also performed to provide in-depth understanding of the roles of different coatings and the performance-enhancement mechanism. ~~and the~~ The designed bilayer or multilayer coating strategy demonstrated in our work provides a promising option for making highly effective electrodes for next-generation LIBs.

2. Experimental

2.1. Synthesis of electrode materials

2.1.1. C-coated Si-SiO_x particles

The C-coated Si-SiO_x particles with a core-shell structure (Si-SiO_x@C) are prepared by pyrolysis of phenolic resin with commercial SiO powder (Fig. 1a). First, a mixture of SiO powder (10.0 g) and phenolic resin (0.75 g) is added into a milling pot (of 100 mL). After ball milling (with zirconia balls) at a low rotational speed (200 rpm) for 1 h, the mixture is carbonized under N₂ atmosphere in a tube furnace. The carbonization process involves a pre-annealing treatment (200 °C for 2 h) and a subsequent calcination at elevated temperatures (800 °C, 900 °C, or 1000 °C for 2 h plus a furnace cooling). During the second step, SiO will undergo disproportionation:



The synthesized Si-SiO_x@C particles are denoted as Si-SiO_x@C⁸⁰⁰, Si-SiO_x@C⁹⁰⁰, and Si-SiO_x@C¹⁰⁰⁰ according to their calcination temperatures. Because 900 °C is found to be the best for preparing C coatings from phenolic resin, Si-SiO_x@C hereinafter refers to Si-SiO_x@C⁹⁰⁰. The detailed process for finding the optimized calcination temperature is presented in the Supplementary Materials (Section S1).

2.1.2. Additional PMC coating

The as-prepared Si-SiO_x@C particles (5.85 g) are blended with CNPs (0.15 g) in a solvent containing ethanol (40 mL) and deionized water (40 mL). Then 15 mL polyvinylpyrrolidone (PVP, with a concentration of 5%) and 15 mL pyrrole (10%) are added into the solvent under continuous mechanical agitation. PVP serves as a dispersing agent for the reactant pyrrole which is absorbed on the surface of the C coating under van der Waals force. Two hours later, 10 mL H₂O₂ are added as an oxidizing agent, and followed by another mechanical agitation for 24 h to accomplish the polymerization from pyrrole monomers to polypyrrole (PPy) and the formation of C–O–N bonds as the crosslink **I** between C coating and PPy. Eventually, as illustrated in Fig. 1b, the initial Si-

SiO_x@C particles are coated by additional layer of PMC, namely, CNP reinforced PPy (CNP-PPy), and the resultant products are denoted as Si-SiO_x@C/CNP-PPy (also in Fig. 1c), which are collected by centrifuging and subsequent vacuum drying for 12 h.

The morphology and grain size of the SiO raw material and the as-prepared Si-SiO_x@C and Si-SiO_x@C/CNP-PPy micro-particles are very similar with an average grain size less than 10 μm, as revealed by scanning electron microscopy (SEM) (Fig. S3 in the Supplementary Materials).

2.2. Battery assembly

For assembling a half cell (of 2025 coin-type), its working electrode is fabricated by mixing as-prepared particles (1.2 g) as the active materials, acetylene black (0.15 g), and Poly(acrylic acid) (PAA) solution (3 g with a concentration of 5%) which serves as the binder, with a weight ratio of 8 : 1 : 1. This mixture is coated onto a copper foil and vacuum dried at 150 °C for 5 h, during which a crosslink reaction (crosslink II) between PPy and PAA occurs, as demonstrated by the blue dotted squares in Fig. 1c. The electrolyte is LiPF₆ (1 M) in fluoroethylene carbonate, polycarbonate, and diethyl carbonate (1 : 1 : 4, v%) with an additive of 1 wt.% vinylene carbonate. A membrane (Celgard 2400) is used as the separator. All half cells are assembled in an argon-filled glovebox.

To preliminarily measure the charging/discharging voltage window of the electrode materials in a full cell (of pouch-type), we first assemble a three-electrode cell. The assembling procedures and preliminary measurement results of both the three-electrode and full cells are detailed in Section S3. Further details about material characterization are available in Section S4.

3. Results and discussion

Electrodes made of the Si-SiO_x@C/CNP-PPy micro-particles exhibit remarkable

long-term cycling performance for both half and full cells. As shown in Fig. 2a, the reversible capacity of the half cell after more than 900 cycles is as high as 800 mAh/g, and its CE value remains almost 100%. This cycling performance is outstanding compared to recent reports on Si-based electrodes in coin-type half cells [19, 22, 26, 27, 37, 38, 44-50], as summarized in Table S2 (Section S5 in the Supplementary Materials).

Fig. 2b shows the long-term cycling performance of a Si-SiO_x@C/CNP-PPy full cell compared to a conventional graphite (as the anode) full cell. The Si-SiO_x@C/CNP-PPy cell has an initial energy density of about 308 Wh/kg and remains 278 Wh/kg after 1118 cycles, which are higher than those of the graphite-based cell. Compared to recent reports on rechargeable pouch-type full cells using Si-based anodes [24, 25, 36, 51], as summarized in Table S3 (in Section S6), our assembled full cell ranks the best in terms of cycling stability. Moreover, the excellent performance of the Si-SiO_x@C/CNP-PPy electrodes demonstrated in Fig. 2 enables us to assemble a full battery which can successfully power a car model (Movies S1–S2 in Supplementary Materials), further demonstrating its potential application in commercial LIBs.

The excellent cycling performance of the half and full cells is attributed to the high structural stability of the fabricated Si-SiO_x@C/CNP-PPy micro-particles. Fig. 2c is an SEM image of the as-prepared electrode, with the bright regions being the Si-SiO_x@C/CNP-PPy particles and the dark regions being graphite. The inset gives a typical grain-size distribution of the synthesized micro-particles, showing that the majority of these particles has a grain size about 6 μm with a small portion of finer ones about 0.6 μm. When assembling batteries, the coarse particles can form void spaces that the fine particles can fill in. As a consequence, this combination of coarse and fine particles is beneficial for obtaining densely packed electrodes with high mass loading and specific capacity. After the full battery cycling (1118 cycles), the electrode still shows coarse

particles without apparent pulverization (Fig. 2e). X-ray diffraction (XRD) of both pre- and post-cycling electrodes (Fig. S7) further indicates little change in their component phases, except for a small amount of Li_2CO_3 formed after cycling (Section S7) [52]. The relatively rough surface of the particles after long-term cycling (Fig. 2f) is attributed to the formation of a stable SEI layer. Some cracks are also visible (Fig. 2e and magnified in Fig. 2f) owing to the inevitable change in particle volume during cycling, which can induce larger SEI layers and more Li^+ consumption. This explains the relatively faster decay of energy density for the $\text{SiO}_x\text{@C/CNP-PPy}$ full cell compared to the one with the pure graphite anode shown in Fig. 2b. On the other hand, such cracks do not change the overall shape and size of the $\text{SiO}_x\text{@C/CNP-PPy}$ particles after long-term battery cycling, which demonstrates high structural stability.

To better understand the underlying mechanism of the observed performance and structural stability enhancement, we have carried out a systematic characterization of a group of Si-based micro-particles with different cores and coatings, namely, SiO , SiO@CNP-PPy , $\text{Si-SiO}_x\text{@C}$, $\text{Si-SiO}_x\text{@C/PPy}$, and $\text{Si-SiO}_x\text{@C/CNP-PPy}$ (detailed synthesis conditions are given in Section S8). Their half-cell performances are summarized in Fig. 3. From the first charging/discharging cycle at a rate of 0.1 C (Fig. 3a), the Si-containing micro-particles all manifest higher initial charge capacity (CC) and CE than those without Si (i.e., SiO and SiO@CNP-PPy , also refer to Table S1). This is not a surprise given the higher theoretical capacity of the crystalline Si compared to SiO . The existence of crystalline Si is identified explicitly by XRD shown in Fig. 3e, in which the diffraction peaks of Si are indexed and the wide peak at about 22.4° corresponds to amorphous SiO_x [11, 15]. High-resolution transmission electron microscopy (TEM) imaging further reveals the core structure to be nanocrystalline Si (nc-Si) embedded in amorphous SiO_x matrix (Fig. S8). Such a Si- SiO_x mixed system combines the high energy

density of Si with the smaller volumetric expansion of SiO_x , offering an ideal candidate for high-capacity LIB electrodes. The beneficial role of Si is also reflected in the cycling performance (20 cycles at 0.1 C rate) shown in Fig. 3b, in which the Si-containing micro-particles all have larger capacity retention than those without Si.

We note that the presence of C coating may also contribute to the better performance of the Si-containing samples shown in Figs. 3a and 3b. Fig. 3c presents the electrochemical impedance spectroscopy (EIS) measurements of the micro-particles, among which those with C coating (i.e., $\text{Si-SiO}_x@\text{C}$, $\text{Si-SiO}_x@\text{C/PPy}$, and $\text{Si-SiO}_x@\text{C/CNP-PPy}$) exhibit smaller semi-circle diameters, higher tail slopes, and hence better charge-transfer performance [53-56]. The presence of C coating can be detected by the two characteristic peaks in Raman spectra (D & G in Fig. 3f). Scanning TEM also reveals a continuous C coating ~ 80 nm thick at the micro-particle surface, the composition of which is confirmed by X-ray energy dispersive spectroscopy mapping, as shown in Figs. S9–S10. Furthermore, the intensity ratio I_D/I_G from Raman spectra provides a metric to evaluate the extent of disorder existing in the C coating, with the smaller I_D/I_G indicating less disorder and thus higher extent of graphitization. The I_D/I_G values of the three C-coated micro-particles are 0.96, 0.99, and 1.03 for $\text{Si-SiO}_x@\text{C}$, $\text{Si-SiO}_x@\text{C/CNP-PPy}$, and $\text{Si-SiO}_x@\text{C/PPy}$, respectively. This sequence is also well reflected in Fig. 3d (a magnified image of the semi-circles marked by a dashed-line square in Fig. 3c), in which a rising extent of graphitization (smaller I_D/I_G) in the C coatings enhances the electrical conductivity and charge transfer rate (smaller semi-circle).

With the highest graphitization extent and conductivity achieved in the $\text{Si-SiO}_x@\text{C}$ particles, however, their cycling stability is poor compared to other samples (Fig. 3b), indicating insufficient stability of the C coating alone and the necessity of adding other coatings. Indeed, with the extra PPy coatings, all samples (i.e., $\text{SiO}@ \text{CNP-PPy}$, Si-

SiO_x@C/PPy, and Si-SiO_x@C/CNP-PPy) show much stabler cycling performance, among which the Si-SiO_x@C/CNP-PPy cell exhibits the best performance, proving the superiority of the CNP-PPy coating. This is further demonstrated in the full-cell performance shown in Fig. 4a: the Si-SiO_x@C/CNP-PPy full cell experiences a long period (1118 cycles) to reach a capacity retention of 80%, which is significantly better than that of the Si-SiO_x@C cell without the PPy coating (80% after only 643 cycles). The rate performance of two half cells with and without CNP-PPy coating, as shown in Fig. 4b, also demonstrates the advantage of the bilayer coating. The charging/discharging behaviors of the two half cells in the course of the first three cycles (Figs. 4c–4d) further show that the CNP-PPy coating leads to a stabler CC, and its CE maintains nearly 100% after the 1st cycle. By comparing the cyclic voltammetry (CV) curves (Figs. 4e–4f), it can be seen that the Si-SiO_x@C/CNP-PPy cell manifests clearer reduction peaks at about 0.49, 0.8 and 1.15 V and a much lower oxidation peak at 0.67 V (< 0.75 V in Fig. 4e). In addition, other examination results of full cells using the Si-SiO_x@C/CNP-PPy particles, including EIS measurement, rate performance and corresponding temperature evolution, are all satisfying (Section S11).

Fig. 5a shows a TEM bright-field image of the surface of a Si-SiO_x@C/CNP-PPy particle, in which the dark area is the Si-SiO_x core. No obvious interface is observed between the C and the CNP-PPy coatings. The thickness of the C/CNP-PPy bilayer coating is about 120 nm, which is 1.5 times thicker than the pure C coating (Fig. S9). In a magnified image (Fig. 5b), uniformly distributed CNPs with diameters of only few nanometers can be distinguished in the PPy matrix. Such well-dispersed CNPs should enhance the strength of PPy and improve the mechanical properties of the Si-SiO_x@C/CNP-PPy particles and the electrodes made of them, which is testified unequivocally by nanoindentation shown in Fig. 5c. From the nanoindentation force-

depth curves with the same threshold force (200 mN), adding C coating increases both the Young's modulus (reflected by curve slope) and hardness (reflected by the maximal indentation depth) from pure SiO particles, while the highest Young's modulus and hardness is achieved in the Si-SiO_x@C/CNP-PPy electrode, which is also quantitatively summarized in Fig. 5d. In addition to above strengthening effect, adding CNPs also increases the graphitization extent in the C/PPy-bilayer coating and improves conductivity, as shown in Figs. 3d and 3f.

Besides the reinforcement from well-dispersed CNPs, the enhanced mechanical strength of the bilayer coating can also be attributed to the crosslink bonding formed between various layers. This is revealed by comparing the surface chemical bonding of different particles (SiO, Si-SiO_x@C, and Si-SiO_x@C/CNP-PPy) using X-ray photoelectron spectroscopy (XPS). Their elemental compositions, namely, Si_{2p} (at 103 eV), C_{1s} (285 eV), N_{1s} (400 eV), and O_{1s} (531 eV) are measured as shown in Fig. S14. The high-resolution XPS spectra of Si_{2p}, C_{1s}, and N_{1s} are further analyzed by deconvolution using a Gaussian-Lorentzian mixed function [57]. Fig. 5e shows the Si_{2p} spectra, in which three fitting components located at 100.2, 102.1 and 104 eV are attributed to Si⁰, Si²⁺ and Si⁴⁺ groups, respectively [58, 59]. The measured proportion of the Si²⁺ group reduces from 24.5% in SiO to about 16% in Si-SiO_x@C and Si-SiO_x@C/CNP-PPy, which is owing to the disproportionation reaction (Eq. 1). Fig. 5f displays the C_{1s} spectra where the four components, C-C (284.5 eV), C-O (285.2 eV), C=O (286.9 eV), and O-C=O (289.3 eV) can be identified [39, 60]. The proportions of two oxygen-containing bonds (C=O and C-O) change significantly from Si-SiO_x@C to Si-SiO_x@C/CNP-PPy: C=O bond decreases from 27.2% to 7.7%, whereas C-O bond increases from 21.1% to 41.3%, which evidently shows a transformation from C=O to C-O bonds occurring on the surface of the Si-SiO_x@C particles during the PPy coating

process (refer to Figs. 1b and 1c). Fig. 5g presents the N_{1s} spectrum acquired on a $SiO_x@C/CNP-PPy$ particle. The four components at 399.4, 400.1, 400.9, and 402.1 eV correspond to pyridinic N, pyrrolic N, graphitic N, and N–O groups, respectively [61, 62]. As the majority of the N-related species, the pyrrolic N has been reported to be effective in improving electrical conductivity [61, 63]. The N–O bonds may arise from a crosslink reaction between pyrrole and C=O, which transforms C=O to C–O and forms C–O–N bonds via sp^2 hybridization [61, 63]. The C–O–N bonds so formed act as the crosslink **I** between C coating and PPy (Fig. 1c).

Moreover, when using the bilayer-coated particles to make electrodes, the PAA binder (refer to Section 2.2) plays an important role to provide strong adhesion not only between particles and current collector, but also among the particles themselves. The effect of the PAA binder is testified by comparing the Fourier transform infrared (FTIR) spectrum of the PPy/PAA composite with those of pure PPy and PAA, as shown in Fig. 5h. The peaks at 1556, 1411, 1287, 1261, 1169 cm^{-1} arise from antisymmetric pyrrole ring vibration, symmetric pyrrole ring vibration, N–H bond deformation vibration, carboxyl group (COOH) deformation and stretching, respectively [36, 64]. In contrast to pure PPy and PAA, the PPy/PAA composite has an apparent reduction in the intensity of the peaks related to the N–H bond and COOH group, which reflects a crosslink reaction between the N–H bonds (in PPy) and the COOH groups (in PAA) [65], i.e., the crosslink **II** as illustrated in Fig. 1c. The co-existence of the crosslinks **I** (between the C and PPy coatings) and **II** (between PPy and PAA), together with the dispersed CNPs in PPy matrix, should enhance the mechanical strength of the coating layers significantly as revealed by nanoindentation (Fig. 5c). Such strengthened coating is expected to confine and buffer the volumetric expansion of the micro-particles effectively, and to maintain the integrity of electrodes during charging/discharging cycles, which is responsible for the outstanding

cycling stability of the assembled batteries.

4. Conclusions

We prepare Si-SiO_x micro-particles with bilayer nano-coating via a simple two-step method. The fabricated nanocrystalline Si embedded in SiO_x matrix provides high energy density with compromised volumetric expansion, and is coated with C to increase conductivity and charge transfer rate. We further deposit the CNP-PPy coating with high mechanical strength, originating from the reinforcement of dispersed CNPs in PPy matrix as well as the crosslink bonding formed between the C coating, the PPy coating, and the PAA binder. With such a strengthened CNP-PPy coating to confine the volumetric expansion of Si-SiO_x, the achieved Si-SiO_x@C/CNP-PPy particles exhibit excellent cycling performance of both half and full cells underpinned by their superior structural stability. In particular, its cycling stability with the capacity retention ~80% after over 1100 cycles is among the best ever reported for Si-based electrodes. A full battery using the Si-SiO_x@C/CNP-PPy electrode successfully drives a car model, which demonstrates a bright application prospect of the C/polymer bilayer coating strategy for optimizing the capacity and cycle life of Si-based electrodes.

Acknowledgements

This work is supported by the Research Foundation for Distinguished Scholars of Qingdao Agricultural University (665-1119008), the Hong Kong Research Grants Council through the Early Career Scheme (Project No. 25301617) and the Hong Kong Polytechnic University grant (Project No. 1-ZE6G). The authors would like to thank Dr. Wei Lu for optimizing the JEOL JEM-2100F microscope and also thank the Central Laboratory of Qingdao Agriculture University for the help in material characterization.

References

- [1] A.P. Wang, S. Kadam, H. Li, S.Q. Shi, Y. Qi, Review on modeling of the anode solid electrolyte interphase (SEI) for lithium-ion batteries, *npj Comput. Mater.*, 4 (2018) 15 <https://doi.org/10.1038/s41524-018-0064-0>.
- [2] K. Cao, L. Jiao, H. Liu, Y. Liu, Y. Wang, Z. Guo, H. Yuan, 3D hierarchical porous α - Fe_2O_3 nanosheets for high-performance lithium-ion batteries, *Adv. Energy Mater.*, 5 (2015) 1401421 <https://doi.org/10.1002/aenm.201401421>.
- [3] D. Wang, Y. Yu, H. He, J. Wang, W. Zhou, H.D. Abruña, Template-free synthesis of hollow-structured Co_3O_4 nanoparticles as high-performance anodes for lithium-ion batteries, *ACS Nano*, 9 (2015) 1775-1781 <https://doi.org/10.1021/nn506624g>.
- [4] G. Wang, Y. Sun, D. Li, W. Wei, X. Feng, K. Müllen, Constructing hierarchically hollow core-shell MnO_2/C hybrid spheres for high-performance lithium storage, *Small*, 12 (2016) 3914-3919 <https://doi.org/10.1002/sml.201601403>.
- [5] J. Wang, J. Wu, Z. Wu, L. Han, T. Huang, H.L. Xin, D. Wang, High-rate and long-life lithium-ion battery performance of hierarchically hollow-structured $\text{NiCo}_2\text{O}_4/\text{CNT}$ nanocomposite, *Electrochim. Acta*, 244 (2017) 8-15 <https://doi.org/10.1016/j.electacta.2017.05.092>.
- [6] J. Wang, H. He, Z. Wu, J. Liang, L. Han, H.L. Xin, X. Guo, Y. Zhu, D. Wang, Controllable construction of flower-like $\text{FeS}/\text{Fe}_2\text{O}_3$ composite for lithium storage, *J. Power Sources*, 392 (2018) 193-199 <https://doi.org/10.1016/j.jpowsour.2018.04.107>.
- [7] J.L. Goldman, B.R. Long, A.A. Gewirth, R.G. Nuzzo, Strain anisotropies and self-limiting capacities in single-crystalline 3D silicon microstructures: Models for high energy density lithium-ion battery anodes, *Adv. Funct. Mater.*, 21 (2011) 2412-2422 <https://doi.org/10.1002/adfm.201002487>.

- [8] X.H. Liu, L. Zhong, S. Huang, S.X. Mao, T. Zhu, J.Y. Huang, Size-dependent fracture of silicon nanoparticles during lithiation, *ACS Nano*, 6 (2012) 1522-1531 <https://doi.org/10.1021/nn204476h>.
- [9] M. Zhang, T. Zhang, Y. Ma, Y. Chen, Latest development of nanostructured Si/C materials for lithium anode studies and applications, *Energy Storage Mater.*, 4 (2016) 1-14 <https://doi.org/10.1016/j.ensm.2016.02.001>.
- [10] T. Ma, X. Yu, X. Cheng, H. Li, W. Zhu, X. Qiu, Confined solid electrolyte interphase growth space with solid polymer electrolyte in hollow structured silicon anode for Li-ion batteries, *ACS Appl. Mater. Interfaces*, 9 (2017) 13247-13254 <https://doi.org/10.1021/acsami.7b03046>.
- [11] X. Zhang, X. Qiu, D. Kong, L. Zhou, Z. Li, X. Li, L. Zhi, Silicene flowers: A dual stabilized silicon building block for high-performance lithium battery anodes, *ACS nano*, 11 (2017) 7476-7484 <https://doi.org/10.1021/acs.nano.7b03942>.
- [12] W. Hui, C. Yi, Designing nanostructured Si anodes for high energy lithium ion batteries, *Nano Today*, 7 (2012) 414-429 <https://doi.org/10.1016/j.nantod.2012.08.004>.
- [13] J. Liu, N. Li, M.D. Goodman, H.G. Zhang, E.S. Epstein, B. Huang, Z. Pan, J. Kim, J.H. Choi, X. Huang, Mechanically and chemically robust sandwich-structured C@Si@C nanotube array Li-ion battery anodes, *ACS Nano*, 9 (2015) 1985-1994 <https://doi.org/10.1021/nn507003z>.
- [14] L. Zhang, X. Liu, Q. Zhao, S. Dou, H. Liu, Y. Huang, X. Hu, Si-containing precursors for Si-based anode materials of Li-ion batteries: A review, *Energy Storage Mater.*, 4 (2016) 92-102 <https://doi.org/10.1016/j.ensm.2016.01.011>.
- [15] L. Zong, Y. Jin, C. Liu, B. Zhu, X. Hu, Z. Lu, J. Zhu, Precise perforation and scalable production of Si particles from low grade sources for high performance lithium ion battery anodes, *Nano Lett.*, 16 (2016) 7210-7215 <https://doi.org/10.1021/acs.nanolett.6b03567>.

- [16] N. Lin, Y. Han, J. Zhou, K. Zhang, T. Xu, Y. Zhu, Y. Qian, A low temperature molten salt process for aluminothermic reduction of silicon oxides to crystalline Si for Li-ion batteries, *Energy Environ. Sci.*, 8 (2015) 3187-3191 <https://doi.org/10.1039/c5ee02487k>.
- [17] T. Song, J. Xia, J.H. Lee, D.H. Lee, M.S. Kwon, J.M. Choi, J. Wu, S.K. Doo, H. Chang, W.I. Park, Arrays of sealed silicon nanotubes as anodes for lithium ion batteries, *Nano Lett.*, 10 (2010) 1710-1716 <https://doi.org/10.1021/nl100086e>.
- [18] A. Gao, S. Mukherjee, I. Srivastava, M. Daly, C.V. Singh, Atomistic origins of ductility enhancement in metal oxide coated silicon nanowires for Li-ion battery anodes, *Adv. Mater. Interfaces*, 4 (2017) 1700920 <https://doi.org/10.1002/admi.201700920>.
- [19] S. Sim, P. Oh, S. Park, J. Cho, Critical thickness of SiO₂ coating layer on core@shell bulk@nanowire Si anode materials for Li-ion batteries, *Adv. Mater.*, 25 (2013) 4498-4503 <https://doi.org/10.1002/adma.201301454>.
- [20] K.H. Kim, D.J. Lee, K.M. Cho, S.J. Kim, J.-K. Park, H.-T. Jung, Complete magnesiothermic reduction reaction of vertically aligned mesoporous silica channels to form pure silicon nanoparticles, *Sci. Rep.*, 5 (2015) 9014 <https://doi.org/10.1038/srep09014>.
- [21] M.R. Babaa, A. Moldabayeva, M. Karim, A. Zhexembekova, Y. Zhang, Z. Bakenov, A. Molkenova, I. Taniguchi, Development of a novel SiO₂ based composite anode material for Li-ion batteries, *Mater. Today Proc.*, 4 (2017) 4542-4547 <https://doi.org/10.1016/j.matpr.2017.04.027>.
- [22] S.J. Lee, H.J. Kim, T.H. Hwang, S. Choi, S.H. Park, E. Deniz, D.S. Jung, J.W. Choi, Delicate structural control of Si-SiO_x-C composite via high-speed spray pyrolysis for Li-ion battery anodes, *Nano Lett.*, 17 (2017) 1870-1876 <https://doi.org/10.1021/acs.nanolett.6b05191>.

- [23] T. Yang, X. Tian, X. Li, K. Wang, Z. Liu, Q. Guo, Y. Song, Double core-shell Si@C@SiO₂ for anode material of lithium-ion batteries with excellent cycling stability, *Chem. Eur. J.*, 23 (2017) 2165-2170 <https://doi.org/10.1002/chem.201604918>.
- [24] C. Shen, X. Fang, M. Ge, A. Zhang, Y. Liu, Y. Ma, M. Mecklenburg, X. Nie, C. Zhou, Hierarchical carbon-coated ball-milled silicon: Synthesis and applications in free-standing electrodes and high-voltage full lithium-ion batteries, *ACS Nano*, 12 (2018) 6280-6291 <https://doi.org/10.1021/acsnano.8b03312>.
- [25] C. Li, T. Shi, H. Yoshitake, H. Wang, A flexible high-energy lithium-ion battery with a carbon black-sandwiched Si anode, *Electrochim. Acta*, 225 (2017) 11-18 <https://doi.org/10.1016/j.electacta.2016.12.105>.
- [26] X. Cao, X. Chuan, R.C. Masse, D. Huang, S. Li, G. Cao, A three layer design with mesoporous silica encapsulated by a carbon core and shell for high energy lithium ion battery anodes, *J. Mater. Chem. A*, 3 (2015) 22739-22749 <https://doi.org/10.1039/c5ta05879a>.
- [27] L.Y. Yang, H.Z. Li, J. Liu, Z.Q. Sun, S.S. Tang, M. Lei, Dual yolk-shell structure of carbon and silica-coated silicon for high-performance lithium-ion batteries, *Sci. Rep.*, 5 (2015) 10908 <https://doi.org/10.1038/srep10908>.
- [28] X. Wang, G. Li, H.S. Min, G. Lui, F.M. Hassan, K. Feng, X. Xiao, Z. Chen, Carbon-coated silicon nanowires on carbon fabric as self-supported electrodes for flexible lithium-ion batteries, *ACS Appl. Mater. Interfaces*, 9 (2017) 9551-9558 <https://doi.org/10.1021/acsami.6b12080>.
- [29] Y. Cen, R.D. Sisson, Q. Qin, J. Liang, Current progress of Si/graphene nanocomposites for lithium-ion batteries, *C - J. Carbon Res.*, 4 (2018) 18 <https://doi.org/10.3390/c4010018>.

- [30] I. Ryu, S.W. Lee, H. Gao, Y. Cui, W.D. Nix, Microscopic model for fracture of crystalline Si nanopillars during lithiation, *J. Power Sources*, 255 (2014) 274-282 <https://doi.org/10.1016/j.jpowsour.2013.12.137>.
- [31] H. Xiang, K. Zhang, G. Ji, J.Y. Lee, C. Zou, X. Chen, J. Wu, Graphene/nanosized silicon composites for lithium battery anodes with improved cycling stability, *Carbon*, 49 (2011) 1787-1796 <https://doi.org/10.1016/j.carbon.2011.01.002>.
- [32] W. Li, Y. Tang, W. Kang, Z. Zhang, X. Yang, Y. Zhu, W. Zhang, C.S. Lee, Core-shell Si/C nanospheres embedded in bubble sheet-like carbon film with enhanced performance as lithium ion battery anodes, *Small*, 11 (2015) 1345-1351 <https://doi.org/10.1002/sml.201402072>.
- [33] H.T. Nguyen, F. Yao, M.R. Zamfir, C. Biswas, K.P. So, Y.H. Lee, S.M. Kim, S.N. Cha, J.M. Kim, D. Pribat, Highly interconnected Si nanowires for improved stability Li-ion battery anodes, *Adv. Energy Mater.*, 1 (2011) 1154-1161 <https://doi.org/10.1002/aenm.201100259>.
- [34] J. Yang, J. Xie, X. Zhou, Y. Zou, J. Tang, S. Wang, F. Chen, L. Wang, Functionalized N-doped porous carbon nanofiber webs for a lithium-sulfur battery with high capacity and rate performance, *J. Phys. Chem. C*, 118 (2014) 1800-1807 <https://doi.org/10.1021/jp410385s>.
- [35] S. Goriparti, E. Miele, F.D. Angelis, E.D. Fabrizio, R.P. Zaccaria, C. Capiglia, Review on recent progress of nanostructured anode materials for Li-ion batteries, *J. Power Sources*, 257 (2014) 421-443 <https://doi.org/10.1016/j.jpowsour.2013.11.103>.
- [36] M. Marinaro, D. Yoon, G. Gabrielli, P. Stegmaier, E. Figgemeier, P.C. Spurk, D. Nelis, G. Schmidt, J. Chauveau, P. Axmann, High performance 1.2 Ah Si-alloy/Graphite|LiNi_{0.5}Mn_{0.3}Co_{0.2}O₂ prototype Li-ion battery, *J. Power Sources*, 357 (2017) 188-197 <https://doi.org/10.1016/j.jpowsour.2017.05.010>.

- [37] Y. Liang, L. Cai, L. Chen, X. Lin, R. Fu, M. Zhang, D. Wu, Silica nanonetwork confined in nitrogen-doped ordered mesoporous carbon framework for high-performance lithium-ion battery anodes, *Nanoscale*, 7 (2015) 3971-3975 <https://doi.org/10.1039/c4nr06611a>.
- [38] Z. Sun, F. Xin, C. Cao, C. Zhao, C. Shen, W.-Q. Han, Hollow silica-copper-carbon anodes using copper metal-organic frameworks as skeletons, *Nanoscale*, 7 (2015) 20426-20434 <https://doi.org/10.1039/c5nr04416b>.
- [39] Y.K. Kim, J.W. Moon, J.G. Lee, Y.K. Baek, S.H. Hong, Porous carbon-coated silica macroparticles as anode materials for lithium ion batteries: Effect of boric acid, *J. Power Sources*, 272 (2014) 689-695 <https://doi.org/10.1016/j.jpowsour.2014.08.128>.
- [40] M. Li, W. Wahyudi, P. Kumar, F. Wu, X. Yang, H. Li, L.-J. Li, J. Ming, Scalable approach to construct free-standing and flexible carbon networks for lithium-sulfur battery, *ACS Appl. Mater. Interfaces*, 9 (2017) 8047-8054 <https://doi.org/10.1021/acsami.6b12546>.
- [41] B. Hertzberg, A. Alexeev, G. Yushin, Deformations in Si-Li anodes upon electrochemical alloying in nano-confined space, *J. Am. Chem. Soc.*, 132 (2010) 8548-8549 <https://doi.org/10.1021/ja1031997>.
- [42] H.K. Liu, Z.P. Guo, J.Z. Wang, K. Konstantinov, Si-based anode materials for lithium rechargeable batteries, *J. Mater. Chem.*, 20 (2010) 10055-10057 <https://doi.org/10.1039/c0jm01702g>.
- [43] S. Liang, X. Zhu, P. Lian, W. Yang, H. Wang, Superior cycle performance of Sn@C/graphene nanocomposite as an anode material for lithium-ion batteries, *J. Solid State Chem.*, 184 (2011) 1400-1404 <https://doi.org/10.1016/j.jssc.2011.03.052>.

- [44] J. Liang, X. Li, Y. Zhu, C. Guo, Y. Qian, Hydrothermal synthesis of nano-silicon from a silica sol and its use in lithium ion batteries, *Nano Res.*, 8 (2015) 1497-1504 <https://doi.org/10.1007/s12274-014-0633-6>.
- [45] C. Zhang, L. Gu, N. Kaskhedikar, G. Cui, J. Maier, Preparation of silicon@silicon oxide core-shell nanowires from a silica precursor toward a high energy density Li-ion battery anode, *ACS Appl. Mater. Interfaces*, 5 (2013) 12340-12345 <https://doi.org/10.1021/am402930b>.
- [46] J. Zhang, J. Gu, H. He, M. Li, High-capacity nano-Si@SiO_x@C anode composites for lithium-ion batteries with good cyclic stability, *J. Solid State Electrochem.*, 21 (2017) 2259-2267 <https://doi.org/10.1007/s10008-017-3578-3>.
- [47] Y. Wang, K. Xie, X. Guo, W. Zhou, G. Song, S. Cheng, Mesoporous silica nanoparticles as high performance anode materials for lithium-ion batteries, *New J. Chem.*, 40 (2016) 8202-8205 <https://doi.org/10.1039/c6nj01698g>.
- [48] X. Cao, X. Chuan, S. Li, D. Huang, G. Cao, Hollow silica spheres embedded in a porous carbon matrix and its superior performance as the anode for lithium-ion batteries, *Part. Part. Syst. Charact.*, 33 (2016) 110-117 <https://doi.org/10.1002/ppsc.201500218>.
- [49] D. Jia, K. Wang, J. Huang, Filter paper derived nanofibrous silica-carbon composite as anodic material with enhanced lithium storage performance, *Chem. Eng. J.*, 317 (2017) 673-686 <https://doi.org/10.1016/j.cej.2017.02.109>.
- [50] H. He, W. Fu, H. Wang, H. Wang, C. Jin, H.J. Fan, Z. Liu, Silica-modified SnO₂-graphene “slime” for self-enhanced li-ion sbattery anode, *Nano Energy*, 34 (2017) 449-455 <https://doi.org/10.1016/j.nanoen.2017.03.017>.
- [51] C. Li, C. Liu, W. Wang, Z. Mutlu, J. Bell, K. Ahmed, R. Ye, M. Ozkan, C.S. Ozkan, Silicon derived from glass bottles as anode materials for lithium ion full cell batteries, *Sci. Rep.*, 7 (2017) 917 <https://doi.org/10.1038/s41598-017-01086-8>.

- [52] S. Leroy, F. Blanchard, R. Dedryvère, H. Martinez, B. Carré, D. Lemordant, D. Gonbeau, Surface film formation on a graphite electrode in Li-ion batteries: AFM and XPS study, *Surf. Interface Anal.*, 37 (2005) 773-781 <https://doi.org/10.1002/sia.2072>.
- [53] K. Feng, W. Ahn, G. Lui, H.W. Park, A.G. Kashkooli, G. Jiang, X. Wang, X. Xiao, Z. Chen, Implementing an in-situ carbon network in Si/reduced graphene oxide for high performance lithium-ion battery anodes, *Nano Energy*, 19 (2016) 187-197 <https://doi.org/10.1016/j.nanoen.2015.10.025>.
- [54] Q. Xu, J.-Y. Li, J.-K. Sun, Y.-X. Yin, L.-J. Wan, Y.-G. Guo, Watermelon-inspired Si/C microspheres with hierarchical buffer structures for densely compacted lithium-ion battery anodes, *Adv. Energy Mater.*, 7 (2017) 1601481 <https://doi.org/10.1002/aenm.201601481>.
- [55] X. Xiao, W. Zhou, Y. Kim, I. Ryu, M. Gu, C. Wang, G. Liu, Z. Liu, H. Gao, Regulated breathing effect of silicon negative electrode for dramatically enhanced performance of Li-ion battery, *Adv. Funct. Mater.*, 25 (2015) 1426-1433 <https://doi.org/10.1002/adfm.201403629>.
- [56] G. Hou, B. Cheng, Y. Cao, M. Yao, B. Li, C. Zhang, Q. Weng, X. Wang, Y. Bando, D. Golberg, Scalable production of 3D plum-pudding-like Si/C spheres: Towards practical application in Li-ion batteries, *Nano Energy*, 24 (2016) 111-120 <https://doi.org/10.1016/j.nanoen.2016.04.014>.
- [57] H. Shinotsuka, H. Yoshikawa, R. Murakami, K. Nakamura, H. Tanaka, K. Yoshihara, Automated information compression of XPS spectrum using information criteria, *J. Electron Spectrosc. Relat. Phenom.*, (2019) 146903 <https://doi.org/10.1016/j.elspec.2019.146903>.
- [58] N. Umirov, D.-H. Seo, T. Kim, H.-Y. Kim, S.-S. Kim, Microstructure and electrochemical properties of rapidly solidified Si–Ni alloys as anode for lithium-ion

- batteries, J. Ind. Eng. Chem., 71 (2019) 351-360
<https://doi.org/10.1016/j.jiec.2018.11.046>.
- [59] J. Zhang, J. Tang, X. Zhou, M. Jia, Y. Ren, M. Jiang, T. Hu, J. Yang, Optimized porous Si/SiC composite spheres as high-performance anode material for lithium-ion batteries, ChemElectroChem, 6 (2019) 450-455 <https://doi.org/10.1002/celec.201801313>.
- [60] D.-C. Guo, F. Han, A.-H. Lu, Porous carbon anodes for a high capacity lithium-ion battery obtained by incorporating silica into benzoxazine during polymerization, Chem. Eur. J., 21 (2015) 1520-1525 <https://doi.org/10.1002/chem.201405068>.
- [61] R. Lv, T. Cui, M.-S. Jun, Q. Zhang, A. Cao, D.S. Su, Z. Zhang, S.-H. Yoon, J. Miyawaki, I. Mochida, F. Kang, Open-ended, N-doped carbon nanotube-graphene hybrid nanostructures as high-performance catalyst support, Adv. Funct. Mater., 21 (2011) 999-1006 <https://doi.org/10.1002/adfm.201001602>.
- [62] L. Zhao, Y.-S. Hu, H. Li, Z. Wang, L. Chen, Porous Li₄Ti₅O₁₂ coated with N-doped carbon from ionic liquids for Li-ion batteries, Adv. Mater., 23 (2011) 1385-1388 <https://doi.org/10.1002/adma.201003294>.
- [63] P. Iamprasertkun, A. Krittayavathananon, M. Sawangphruk, N-doped reduced graphene oxide aerogel coated on carboxyl-modified carbon fiber paper for high-performance ionic-liquid supercapacitors, Carbon, 102 (2016) 455-461 <https://doi.org/10.1016/j.carbon.2015.12.092>.
- [64] A. Bozkurt, W.H. Meyer, G. Wegner, PAA/imidazol-based proton conducting polymer electrolytes, J. Power Sources, 123 (2003) 126-131 [https://doi.org/10.1016/S0378-7753\(03\)00560-3](https://doi.org/10.1016/S0378-7753(03)00560-3).
- [65] B.G. Kim, Y.S. Kim, Y.H. Kim, H. Kim, Y.J. Hong, H.M. Jung, J.C. Won, Nano-scale insulation effect of polypyrrole/polyimide core-shell nanoparticles for dielectric

composites, Compos. Sci. Technol., 129 (2016) 153-159
<https://doi.org/10.1016/j.compscitech.2016.04.028>.

Figure captions

Fig. 1. A schematic of the experimental procedure for synthesizing C/polymer bilayer coated Si-SiO_x electrode materials: (a) Si-SiO_x@C particles, (b) Si-SiO_x@C/CNP-PPy particles, (c) Interaction of particles with PAA binder when fabricating a working electrode.

Fig. 2. Cycling performance of the Si-SiO_x@C/CNP-PPy half cell (a) and two full cells (b). After the full-cell cycling (1118 cycles), the SEM images display a comparison between the pre- (c) and post-~~eyeling-cycled~~ (e) ~~of the~~ Si-SiO_x@C/CNP-PPy electrodes; (d) and (f) show a single as-prepared and post-~~eyeling-cycled~~ Si-SiO_x@C/CNP-PPy particle, respectively.

Fig. 3. A systematic characterization of a group of Si-based micro-particles with different cores and coatings, namely, SiO, SiO@CNP-PPy, Si-SiO_x@C, Si-SiO_x@C/PPy, Si-SiO_x@C/CNP-PPy, and their half-cell performances: (a) the first charging/discharging cycle, (b) cycling performance for the first 20 cycles, (c) Nyquist plots with the equivalent circuit drawn in Fig. S2f, (d) a magnified image of the area marked by a dashed-line square in (c), (e) XRD, and (f) Raman spectra.

Fig. 4. A comparison of the electrochemical performances of the Si-SiO_x@C and Si-SiO_x@C/CNP-PPy electrodes in half and full cells: (a) cycling performance of two full cells, (b) rate performance of two half cells, (c–d) galvanostatic charging/discharging behaviors of two half cells in the course of their first three cycles, (e–f) CV curves of two half cells. In figure (b), the obviously faster decay of capacity at small current (0.05 C) than at large current (> 0.05 C) is attributed to the formation of an SEI layer over the initial few cycles. In figures (c–d), the 1st discharging cycle contains three voltage-drop procedures: From 0.8 to 0.3 V exhibits a steep fall in the discharging voltage, which may be due to the decomposition of electrolyte and the formation of an SEI layer; From 0.3 to

about 0.2 V may be associated with an irreversible formation of Li_2O or Li_4SiO_4 , which results in a decreased CC after the 1st cycle [26, 47]; From about 0.2 to 0.005 V, two reversible battery reactions produce $\text{Li}_{3.75}\text{Si}$ and Li_6C , which are $\text{SiO}_x + (3.75 + 0.0625x) \text{Li} \leftrightarrow (1 - 0.25x) \text{Li}_{3.75}\text{Si} + 0.25x \text{Li}_4\text{SiO}_4$ and $\text{C} + 6\text{Li} \leftrightarrow \text{Li}_6\text{C}$, respectively [12, 35]. The higher reversibility of these two reactions, the higher values of the battery's CE. In figures (e–f), during the 1st cycle, the peak at 0.49 V may be attributed electrochemical reduction of either SiO_2 or other oxygen-containing groups [26], and the peaks at 0.8 and 1.15 V are due to the formation of an SEI layer and some side reactions happened at electrode/electrolyte interface [32, 46]; during the 3rd cycle, the peak at 0.75 V in figure (e) or 0.67 V in figure (f) is related to Li^+ deintercalation.

Fig. 5. (a) TEM bright-field image of the surface of a $\text{Si-SiO}_x@\text{C}/\text{CNP-PPy}$ particle, (b) a TEM image showing CNPs embedded in PPy matrix, (c) nanoindentation force-depth curves of three working electrodes prepared by different particles and (d) the corresponding Young's modulus and hardness obtained from (c), (e–f) high-resolution XPS spectra of Si_{2p} , C_{1s} , and N_{1s} , respectively, obtained from the surface of different particles, (h) a comparison between the FTIR spectra of pure PPy, PAA, and PPy/PAA composite, among which the pure PPy is produced through an oxidation process described in Section 2.1.2, and the PPy/PAA composite is prepared by mixing the pure PPy and PAA powder with a weight ratio of 1.6 : 1 in ethanol by mechanical agitation for at least 24 h, followed by vacuum drying at 150 °C for 5h.